

A comparison of different order hybrid finite difference-volume methods for solving the Serre equations in conservative law form

Jordan Pitt,¹
Christopher Zoppou,¹
Stephen G. Roberts,¹

ABSTRACT

In this paper first-, second- and third-order accurate numerical methods for solving the Serre equations are described. The method is described as a finite difference-volume method because it uses a finite difference approximation and a finite volume method to solve the Serre equations in conservation law form. These models are validated and used to investigate a conjecture in the literature about the results of solving the Serre equations in the presence of steep gradients. To adequately resolve dispersive waves efficiently in problems containing steep gradients a scheme is required to be at least a second-order accurate.

Keywords: dispersive waves, conservation laws, Serre equations, finite volume method, finite difference method

¹ INTRODUCTION

Free surface flows occur in many important applications such as; tsunamis, storm surges and tidal bores. Because fluid viscosity has a negligible effect on these problems they can be modelled by the Euler equations. However, numerical methods for the Euler equations are not yet computationally efficient enough to deal with these problems over large domains. Thus various approximations to the Euler equations have been derived, one of the crudest is the shallow water wave (SWW) equations which have been used to model free surface flows in the past. However, the SWW equations assume a hydrostatic pressure distribution in a fluid column which is not fully justified in rapidly varying flows

¹Mathematical Sciences Institute, Australian National University, Canberra, ACT 0200, Australia, E-mail: Jordan.Pitt@anu.edu.au. The work undertaken by the first author was supported financially by an Australian National University Scholarship.

10 because vertical acceleration of the fluid particles becomes important. It is the vertical
11 acceleration of these particles that produces a non-hydrostatic pressure distribution and
12 dispersive waves which are not present in the SWW equations. Consequently, many equa-
13 tions have been derived as approximations to the Euler equations in shallow fluids that are
14 less restrictive in their assumptions than the SWW equations. The Serre equations are one
15 of these approximations to the Euler equations and are of particular interest because they
16 do not enforce a hydrostatic pressure distribution over a fluid column allowing for fully
17 non-linear and weakly dispersive flows (Lannes and Bonneton 2009).

18 The Serre equations were first derived by Serre (1953) for flat bottom topographies in
19 one dimension. More general equations were then derived for smooth bottom topographies
20 in one dimension (Su and Gardner 1969) and later smooth bottom topographies in two di-
21 mensions (Green and Naghdi 1976). These equations have been handled in many different
22 ways (Mitsotakis et al. 2014; Bonneton et al. 2011; Antunes do Carmo et al. 1993; Chazel
23 et al. 2011; Cienfuegos and Bonneton 2006; Cienfuegos and Bonneton 2007; Dutykh et al.
24 2011). This paper follows the decomposition of the Serre equations into conservative law
25 form (Le Métayer et al. 2010; Li et al. 2014; Zoppou 2014) and follows the formulation
26 of Le Métayer et al. (2010) and Zoppou (2014). First-, second- and third-order accurate
27 numerical methods are developed for solving the Serre equations in conservation law form.

28 Zoppou and Roberts (1996) demonstrated that first- and third-order methods produce
29 diffusive errors smearing steep gradients. While second-order methods produce dissipative
30 errors introducing non-physical oscillations around steep gradients. Because steep
31 gradients arise naturally in fluid flows and the Serre equations produce dispersive waves
32 (El et al. 2006) it is important that physical oscillations described by the dispersive terms
33 are not significantly polluted by either diffusion or dissipation.

34 This paper aims to clear up the discrepancy between the results of Le Métayer et al.
35 (2010) and El et al. (2006) by examining the behaviour of a certain dam-break problem.
36 In particular, Le Métayer et al. (2010) stated that their first-order method was sufficient to
37 capture the important behaviour of the dam-break problem, this paper will test the validity
38 of that assertion. To accomplish this first-, second- and third-order accurate methods to
39 solve the Serre equations are constructed and validated by comparing the solutions to a
40 known analytical solution to the Serre equations and laboratory data of flows containing
41 steep gradients. Then the validated models are used to resolve this conflict.

42 SERRE EQUATIONS

43 The Serre equations can be derived by integrating the Euler equations over the water
44 depth, as was done by Su and Gardner (1969). They can also be derived from an asymptotic
45 expansion of the Euler equations (Lannes and Bonneton 2009). The former is more
46 consistent with the perspective from which numerical methods will be developed in this

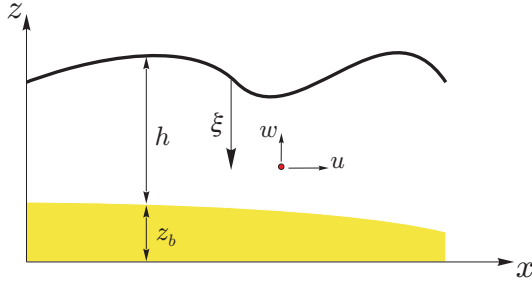


FIG. 1: The notation used for one-dimensional flow governed by the Serre equation.

47 paper while the latter is useful for identifying the appropriate regions in which to use these
48 equations as a model of fluid flow.

49 The scenario under which the Serre approximation is made consists of a two dimensional
50 $\mathbf{x} = (x, z)$ fluid over a variable bathymetry as in Figure 1, under the action of
51 gravity. The water depth is $h(x, t)$ and $z_b(x)$ is the bed elevation. The fluid is subject
52 to the pressure, $p(\mathbf{x}, t)$ and gravitational acceleration, $\mathbf{g} = (0, g)^T$ and has a velocity
53 $\mathbf{v} = (u(\mathbf{x}, t), w(\mathbf{x}, t))$, where $u(\mathbf{x}, t)$ is the velocity in the x -coordinate and $w(\mathbf{x}, t)$ is the
54 velocity in the z -coordinate and t is time. Assuming that $z_b(x)$ is constant the Serre equa-
55 tions read (Li et al. 2014; Zoppou 2014)

56
$$\frac{\partial h}{\partial t} + \frac{\partial(\bar{u}h)}{\partial x} = 0, \quad (1a)$$

57

58

59
$$\underbrace{\frac{\partial(\bar{u}h)}{\partial t} + \frac{\partial}{\partial x} \left(\bar{u}^2 h + \frac{gh^2}{2} \right)}_{\text{Shallow Water Wave Equations}} + \underbrace{\frac{\partial}{\partial x} \left(\frac{h^3}{3} \left[\frac{\partial \bar{u}}{\partial x} \frac{\partial \bar{u}}{\partial x} - \bar{u} \frac{\partial^2 \bar{u}}{\partial x^2} - \frac{\partial^2 \bar{u}}{\partial x \partial t} \right] \right)}_{\text{Dispersion Terms}} = 0 \quad (1b)$$

60
$$\underbrace{\qquad\qquad\qquad}_{\text{Serre Equations}}$$

61 where \bar{u} is the depth averaged velocity.

62 Alternative Conservation Law Form of the Serre Equations

63 In Le Métayer et al. (2010) and Zoppou (2014) it is demonstrated that the Serre equa-
64 tions can be rearranged into a conservation law form, by introducing a new conserved
65 quantity

66
$$G = uh - h^2 \frac{\partial h}{\partial x} \frac{\partial u}{\partial x} - \frac{h^3}{3} \frac{\partial^2 u}{\partial x^2}. \quad (2)$$

67

68 Consequently, (1) can be rewritten as

$$69 \quad 70 \quad \frac{\partial h}{\partial t} + \frac{\partial(uh)}{\partial x} = 0 \quad (3a)$$

71 and

$$72 \quad 73 \quad \frac{\partial G}{\partial t} + \frac{\partial}{\partial x} \left(Gu + \frac{gh^2}{2} - \frac{2h^3}{3} \frac{\partial u}{\partial x} \frac{\partial u}{\partial x} \right) = 0 \quad (3b)$$

74 where the bar over u has been dropped to simplify the notation. A hybrid method can be
 75 developed for the Serre equations that solves the elliptic problem (2) for u and then the
 76 conservation law (3) for h and G . This replicates the process of Le Métayer et al. (2010)
 77 and Zoppou (2014).

78 NUMERICALLY SOLVING THE SERRE EQUATIONS WRITTEN IN 79 CONSERVATION LAW FORM

80 There are numerous ways a numerical method could be built to solve the Serre equa-
 81 tions in conservation law form (3). For flows that contain steep gradients the finite volume
 82 method seems the most appropriate. A finite volume method to solve (3) updates the
 83 conserved quantities h and G over a single time step $\Delta t = t^{n+1} - t^n$. So that

$$84 \quad 85 \quad \begin{bmatrix} h^{n+1} \\ G^{n+1} \end{bmatrix} = \mathcal{L}(h^n, G^n, u^n, \Delta t) \quad (4)$$

86 where \mathcal{L} is some numerical solver for (3) and the superscript denotes the time at which a
 87 quantity is evaluated; e.g. $u^n = u(t^n)$. The complete solution also involves solving (2) for
 88 u given h and G denoted by

$$88 \quad u^{n+1} = \mathcal{A}(h^{n+1}, G^{n+1}). \quad (5)$$

91

92 SOLVING THE ELLIPTIC EQUATION \mathcal{A} FOR U

93 Assuming that a discretisation in space has a fixed resolution so that $\forall i x_{i+1} - x_i =$
 94 Δx ; allows for a simple finite difference approximation to (2) as a suitable method for
 95 \mathcal{A} (Le Métayer et al. 2010; Zoppou 2014). Since the goal of this paper is to develop
 96 and compare a range of different order accurate methods for this problem both a second-
 97 and fourth-order centred finite difference approximation to (2) were used. By taking such
 98 approximations to the first- and second-order spatial derivatives the second- and fourth-
 99 order analogues of (2) are given by

$$100 \quad 101 \quad G_i = u_i h_i - h_i^2 \left(\frac{h_{i+1} - h_{i-1}}{2\Delta x} \right) \left(\frac{u_{i+1} - u_{i-1}}{2\Delta x} \right) - \frac{h_i^3}{3} \left(\frac{u_{i+1} - 2u_i + u_{i-1}}{\Delta x^2} \right) \quad (5a)$$

102 and

$$G_i = u_i h_i - h_i^2 \left(\frac{-h_{i+2} + 8h_{i+1} - 8h_{i-1} + h_{i-2}}{12\Delta x} \right) \left(\frac{-u_{i+2} + 8u_{i+1} - 8u_{i-1} + u_{i-2}}{12\Delta x} \right) - \frac{h_i^3}{3} \left(\frac{-u_{i+2} + 16u_{i+1} - 30u_i + 16u_{i-1} - u_{i-2}}{12\Delta x^2} \right) \quad (5b)$$

105 where the subscript denotes the spatial coordinate at which the quantity is evaluated; e.g.
 106 $u_i = u(x_i)$. Both of these can be rearranged into a matrix equation with the following form

$$\begin{bmatrix} u_0 \\ \vdots \\ u_m \end{bmatrix} = A^{-1}(h) \begin{bmatrix} G_0 \\ \vdots \\ G_m \end{bmatrix} =: \mathcal{A}(h, G)$$

where for a second-order approximation the matrix $A(h)$ is tri-diagonal while for a fourth-order method it is penta-diagonal.

111 SOLVING THE CONSERVATION LAW FORM OF THE SERRE EQUATIONS

112 A finite volume method of sufficient order was developed to solve (3). Unlike finite
 113 difference methods which utilise nodal values of quantities, finite volume methods use the
 114 cell averages, for example the average water depth over a cell which spans $[x_{i-1/2}, x_{i+1/2}]$
 115 is

$$\bar{h}_i = \frac{1}{\Delta x} \int_{x_{i-\frac{1}{2}}}^{x_{i+\frac{1}{2}}} h(x, t) dx$$

where $x_{i\pm 1/2} = x_i \pm \Delta x/2$. Finite volume methods update the cell averages using

$$\bar{U}_i^{n+1} = \bar{U}_i^n - \frac{\Delta t}{\lambda x} \left(F_{i+\frac{1}{2}}^n - F_{i-\frac{1}{2}}^n \right) \quad (6)$$

where $\bar{U}_i^n = [\bar{h}_i^n \ \bar{G}_i^n]^T$ is an approximation of the vector of the conserved quantities averaged over the cell at time t^n . While $F_{i\pm 1/2}^n$ is an approximation of the average flux over the time interval $[t^n, t^{n+1}]$ at the respective cell boundary $x_{i\pm 1/2}$, which is obtained by solving a local Riemann problem at the cell boundaries.

125 Local Riemann Problem

Since \bar{U}_i^n is known for all i what remains is to calculate the time averaged fluxes $F_{i\pm 1/2}$ in (6). In Kurganov et al. (2002) the time averaged inter-cell flux is approximated by

$$F_{i+\frac{1}{2}} = \frac{a_{i+\frac{1}{2}}^+ f(q_{i+\frac{1}{2}}^-) - a_{i+\frac{1}{2}}^- f(q_{i+\frac{1}{2}}^+)}{a_{i+\frac{1}{2}}^+ - a_{i+\frac{1}{2}}^-} + \frac{a_{i+\frac{1}{2}}^+ a_{i+\frac{1}{2}}^-}{a_{i+\frac{1}{2}}^+ - a_{i+\frac{1}{2}}^-} \left[q_{i+\frac{1}{2}}^+ - q_{i+\frac{1}{2}}^- \right] \quad (7)$$

130 where f is the instantaneous flux of the conserved quantity q evaluated using the recon-
 131 structed values from the cells adjacent to the cell interface $x_{i+1/2}$. While $a_{i+1/2}^-$ and $a_{i+1/2}^+$
 132 are given by

$$133 \quad 134 \quad a_{i+\frac{1}{2}}^- = \min \left[\lambda_1 \left(q_{i+\frac{1}{2}}^- \right), \lambda_1 \left(q_{i+\frac{1}{2}}^+ \right), 0 \right]$$

135 and

$$136 \quad 137 \quad a_{i+\frac{1}{2}}^+ = \max \left[\lambda_2 \left(q_{i+\frac{1}{2}}^- \right), \lambda_2 \left(q_{i+\frac{1}{2}}^+ \right), 0 \right]$$

138 where λ_1 and λ_2 are estimates of the smallest and largest eigenvalues respectively of the
 139 Jacobian, $\partial f / \partial u$.

140 Propagation Speeds of a Local Shock

141 As demonstrated in Zoppou (2014) λ_1 and λ_2 are bounded by the phase speed of the
 142 shallow water wave equations, so that

$$143 \quad \lambda_1 := u - \sqrt{gh} \leq v_p \leq u + \sqrt{gh} =: \lambda_2$$

144 where v_p is the phase speed of the Serre equations, thus $a_{i+1/2}^-$ and $a_{i+1/2}^+$ are fully deter-
 145 mined.

146 Reconstruction

147 The quantities $q_{i+1/2}^-$ and $q_{i+1/2}^+$ in (7) are given by the two reconstructions at $x_{i+1/2}$,
 148 one from the cell to the left $[x_{i-1/2}, x_{i+1/2}]$ and one from the cell to the right $[x_{i+1/2}, x_{i+3/2}]$
 149 denoted by the superscripts $-$ and $+$ respectively. The order of the polynomials used to
 150 reconstruct the quantities inside the cells determines the spatial order of accuracy. Constant
 151 polynomials result in a first-order method (Godunov 1959). Similarly first- and second-
 152 degree polynomials result in second- and third-order methods respectively.

153 For a zero-degree polynomial the interpolant has the value \bar{q}_i at x_i , this is also the
 154 case for linear interpolation functions. For the zero-degree case the interpolants are fully
 155 determined i.e $q_{i-1/2}^+ = \bar{q}_i = q_{i+1/2}^-$ and monotinicity preserving. There are a variety of
 156 ways to construct higher-degree interpolants not all of which are necessarily monotonicity
 157 preserving, which can result in the introduction of numerical oscillations during the re-
 158 construction process. To suppress these non-physical oscillations in higher order methods
 159 limiting must be implemented. For the second-order method the minmod limiter was used
 160 as in Kurganov et al. (2002). While for the third-order method the Koren limiter was used
 161 (Koren 1993). This results in the following reconstruction scheme for the second-order
 162 method

$$164 \quad 165 \quad q_{i+\frac{1}{2}}^- = \bar{q}_i + a_i \frac{\Delta x}{2}$$

166 and

$$167 \quad q_{i+\frac{1}{2}}^+ = \bar{q}_{i+1} - a_{i+1} \frac{\Delta x}{2}$$

$$168$$

169 where

$$170 \quad a_i = \text{minmod} \left\{ \theta \frac{\bar{q}_{i+1} - \bar{q}_i}{\Delta x}, \frac{\bar{q}_{i+1} - \bar{q}_{i-1}}{2\Delta x}, \theta \frac{\bar{q}_i - \bar{q}_{i-1}}{\Delta x} \right\} \quad \text{for } \theta \in [1, 2].$$

$$171$$

172 While for the third-order method the reconstruction scheme is

$$173 \quad q_{i+\frac{1}{2}}^- = \bar{q}_i + \frac{1}{2} \phi^-(r_i) (\bar{q}_i - \bar{q}_{i-1})$$

$$174$$

175 and

$$176 \quad q_{i+\frac{1}{2}}^+ = \bar{q}_{i+1} - \frac{1}{2} \phi^+(r_{i+1}) (\bar{q}_{i+1} - \bar{q}_i)$$

$$177$$

178 where

$$179 \quad \phi^-(r_i) = \max \left[0, \min \left[2r_i, \frac{1+2r_i}{3}, 2 \right] \right],$$

$$180$$

$$181$$

$$182 \quad \phi^+(r_i) = \max \left[0, \min \left[2r_i, \frac{2+r_i}{3}, 2 \right] \right]$$

$$183$$

184 and

$$185 \quad r_i = \frac{\bar{q}_{i+1} - \bar{q}_i}{\bar{q}_i - \bar{q}_{i-1}}.$$

$$186$$

187 Fully discrete approximations to the instantaneous flux $f(q_{i+\frac{1}{2}}^\pm)$

188 For water depth, the fully discrete approximation to $f(h_{i+1/2}^\pm)$ in (3a) is given by

$$189 \quad f\left(h_{i+\frac{1}{2}}^\pm\right) = u_{i+\frac{1}{2}}^\pm h_{i+\frac{1}{2}}^\pm$$

$$190$$

191 which is independent of the order of accuracy of the method.

192 The flux $f(G_{i+1/2}^\pm)$ is more complicated because of the derivative term in (3b) and is
193 given by

$$194 \quad f\left(G_{i+\frac{1}{2}}^\pm\right) = u_{i+\frac{1}{2}}^\pm G_{i+\frac{1}{2}}^\pm + \frac{g\left(h_{i+\frac{1}{2}}^\pm\right)^2}{2} - \frac{2\left(h_{i+\frac{1}{2}}^\pm\right)^3}{3} \left[\left(\frac{\partial u}{\partial x} \right)_{i+\frac{1}{2}}^\pm \right]^2.$$

$$195$$

196 The first- and third-order approximations to the derivative term can be obtained by an
 197 upwind finite difference approximation. By assuming that u is continuous, a second-order
 198 approximation that has the correct order and is simpler to implement than its corresponding
 199 upwind finite difference approximation can be used. Thus the following approximations
 200 to the derivatives were obtained, for the first-order method

$$201 \quad \left(\frac{\partial u}{\partial x} \right)_{i+\frac{1}{2}}^+ = \frac{u_{i+\frac{3}{2}}^+ - u_{i+\frac{1}{2}}^+}{\Delta x}$$

$$202$$

203 and

$$204 \quad \left(\frac{\partial u}{\partial x} \right)_{i+\frac{1}{2}}^- = \frac{u_{i+\frac{1}{2}}^- - u_{i-\frac{1}{2}}^-}{\Delta x}.$$

$$205$$

206 For the second-order method

$$207 \quad \left(\frac{\partial u}{\partial x} \right)_{i+\frac{1}{2}}^- = \left(\frac{\partial u}{\partial x} \right)_{i+\frac{1}{2}}^+ = \frac{u_{i+1} - u_i}{\Delta x}$$

$$208$$

209 and for the third-order method

$$210 \quad \left(\frac{\partial u}{\partial x} \right)_{i+\frac{1}{2}}^+ = \frac{-u_{i+\frac{5}{2}}^+ + 4u_{i+\frac{3}{2}}^+ - 3u_{i+\frac{1}{2}}^+}{\Delta x}$$

$$211$$

212 and

$$213 \quad \left(\frac{\partial u}{\partial x} \right)_{i+\frac{1}{2}}^- = \frac{3u_{i+\frac{1}{2}}^- - 4u_{i-\frac{1}{2}}^- + u_{i-\frac{3}{2}}^-}{\Delta x}.$$

$$214$$

215 Transforming between nodal values and cell averages

216 The operator \mathcal{L} given by (6) uses cell averages while the operator \mathcal{A} given by (5a)
 217 and (5b) uses nodal values at the cell centres. Therefore, a transformation from the cell
 218 averages to the nodal values is required. For the first- and second-order methods this
 219 distinction is trivial since $\bar{q}_i = q_i$. However, for the third-order method this is a very
 220 important distinction and failure to handle this correctly will result in a loss of accuracy.

221 A quadratic polynomial that gives the correct cell averages for the cell centred at x_i
 222 and its two neighbours satisfies this equation

$$223 \quad q_i = \frac{-\bar{q}_{i+1} + 26\bar{q}_i - \bar{q}_{i-1}}{24}.$$

$$224$$

225 This is a tri-diagonal matrix equation that transforms from cell averages to nodal values
 226 with third-order accuracy and is denoted by \mathcal{M} . The inverse transformation \mathcal{M}^{-1} denotes
 227 the solution of the tri-diagonal matrix equation given nodal values resulting in cell aver-
 228 ages which is also third-order accurate. For the first- and second-order schemes \mathcal{M} is the
 229 identity matrix. This completes the solution of the Serre equations (2) and (3) with the
 230 following process denoted by \mathcal{H}

231
$$\mathcal{H}(\bar{\mathbf{U}}^n, \Delta t) = \begin{cases} \mathbf{U}^n &= \mathcal{M}(\bar{\mathbf{U}}^n) \\ \mathbf{u}^n &= \mathcal{A}(\mathbf{U}^n) \\ \bar{\mathbf{u}}^n &= \mathcal{M}^{-1}(\mathbf{u}^n) \\ \bar{\mathbf{U}}^{n+1} &= \mathcal{L}(\bar{\mathbf{U}}^n, \bar{\mathbf{u}}^n, \Delta t) \end{cases}.$$

 232

233 **Strong-Stability-Preserving Runge-Kutta Scheme**

234 The process above is first-order accurate in time. This paper will use the strong sta-
 235 bility Runge-Kutta steps described in Gottlieb et al. (2009) to construct fully second- and
 236 third-order accurate methods using linear combinations of \mathcal{H} . This leads to the following
 237 processes, for the first-order method

238
$$\bar{\mathbf{U}}^{n+1} = \mathcal{H}(\bar{\mathbf{U}}^n, \Delta t)$$

 239

240 the second-order method

241
$$\bar{\mathbf{U}}^{(1)} = \mathcal{H}(\bar{\mathbf{U}}^n, \Delta t),$$

 242
$$\bar{\mathbf{U}}^{(2)} = \mathcal{H}(\bar{\mathbf{U}}^{(1)}, \Delta t),$$

 243
$$\bar{\mathbf{U}}^{n+1} = \frac{1}{2}(\bar{\mathbf{U}}^{(1)} + \bar{\mathbf{U}}^{(2)})$$

 244

245 and the third-order method

246
$$\bar{\mathbf{U}}^{(1)} = \mathcal{H}(\bar{\mathbf{U}}^n, \Delta t),$$

 247
$$\bar{\mathbf{U}}^{(2)} = \mathcal{H}(\bar{\mathbf{U}}^{(1)}, \Delta t),$$

 248
$$\bar{\mathbf{U}}^{(3)} = \frac{3}{4}\bar{\mathbf{U}}^n + \frac{1}{4}\bar{\mathbf{U}}^{(2)},$$

 249
$$\bar{\mathbf{U}}^{(4)} = \mathcal{H}(\bar{\mathbf{U}}^{(3)}, \Delta t),$$

 250
$$\bar{\mathbf{U}}^{n+1} = \frac{1}{3}\bar{\mathbf{U}}^n + \frac{2}{3}\bar{\mathbf{U}}^{(4)}.$$

 251

252 **Stability Constraint**

253 A necessary condition for stability of all these explicit methods based on the finite
 254 volume method is the Courant-Friedrichs-Lowy condition (Courant et al. 1928) which
 255 states that for each cell

256
$$\Delta t < \frac{\Delta x}{2 \max(|\lambda_i|)} \forall i. \quad (8)$$

257

258

259 **NUMERICAL SIMULATIONS**

260 The discussed methods will now be used to solve three different problems; (i) the
 261 soliton which is an analytic solution of the Serre equations; (ii) one of the experiments
 262 conducted by Hammack and Segur (1978) and (iii) a dam-break problem from El et al.
 263 (2006) and Le Métayer et al. (2010). The first two will be used to validate the models,
 264 with the soliton used to confirm the order of convergence of the models. The second
 265 problem is used to validate the models using experimental data which contains flows with
 266 steep gradients. Lastly the dam-break problem will be used to compare the results of these
 267 methods with those of El et al. (2006) and Le Métayer et al. (2010). The aim of which is to
 268 verify the claim of the latter that a first-order method for the Serre equations is sufficiently
 269 accurate to capture the important behaviour of the dam-break problem.

270 **Soliton**

271 Currently cnoidal waves are the only family of analytic solutions to the Serre equa-
 272 tions (Carter and Cienfuegos 2011). Solitons are a particular instance of cnoidal waves
 273 that travel without deformation and have been used to verify the convergence rates of the
 274 proposed methods in this paper.

275 For the Serre equations the solitons have the following form

276
$$h(x, t) = a_0 + a_1 \operatorname{sech}^2(\kappa(x - ct)) \quad (9a)$$

and

$$u(x, t) = c \left(1 - \frac{a_0}{h(x, t)} \right) \quad (9b)$$

where

$$\kappa = \frac{\sqrt{3a_1}}{2a_0 \sqrt{a_0 + a_1}} \quad (9c)$$

278 and

$$c = \sqrt{g(a_0 + a_1)} \quad (9d)$$

279 where a_0 and a_1 are input parameters that determine the depth of the quiescent water and
280 the maximum height of the soliton above that respectively. In the simulation $a_0 = 10\text{m}$,
281 $a_1 = 1\text{m}$ for $x \in [-500\text{m}, 1500\text{m}]$ and $t \in [0\text{s}, 100\text{s}]$. With $\Delta t = 0.01\Delta x$ which satisfies (8)
282 and $\theta = 1.2$ for the second-order reconstruction. The example results for $\Delta x = 100/2^6\text{m}$
283 can be seen in Figure 2.

284 Figure 2 demonstrates the superiority of the second- and third-order methods compared
285 to the first-order method. With the first-order method there is significant attenuation of the
286 wave due to its diffusive behaviour which creates a wider wave profile and some smaller
287 trailing waves. However, the first-order method does produce the correct speed of the
288 wave with a small phase error. While the second- and third-order methods demonstrate no
289 noticeable deformation resolving the soliton solution well on a relatively coarse grid with
290 less than 500 cells defining the actual wave.

291 The relative error as measured by the L_1 -norm of the method can be seen in Figure 3.
292 For a vector \mathbf{q} and an approximation to it \mathbf{q}^* the relative error as measured by the L_1 -norm
293 is

$$294 \quad L_1(\mathbf{q}, \mathbf{q}^*) = \frac{\sum_{i=1}^m |q_i - q_i^*|}{\sum_{i=1}^m |q_i|}.$$

295

296 Figure 3 demonstrates that the methods all have the correct order of convergence in
297 both time and space. However, this order of convergence is not uniform over all Δx . When
298 Δx is large the actual problem is not discretised well since the cells are too large to ade-
299 quately resolve the problem; this causes the observed suboptimal rate of convergence in
300 Figure 3. When Δx is sufficiently small the numerical errors become small enough that
301 floating point errors are significant and this can also lead to suboptimal rates of conver-
302 gence as can be seen in Figure 4 which are the convergence results for the third-order
303 method performing a single time step using the same initial conditions and parameters.
304 Thus the suboptimal rates for the third-order method in Figure 3(c) at small Δx are the
305 result of floating point errors. Therefore, the order of convergence for all methods is con-
306 firmed.

307 Figure 3 also demonstrates the superiority of the second- and third-order methods over
308 the first-order method for accuracy. The third-order method is also better than the second-
309 order method in this respect although this difference is less pronounced. These differences
310 have a significant impact on run-time if one wishes to run a simulation up to a desired
311 accuracy. A comparison of the methods for such a problem is presented in Table 1.

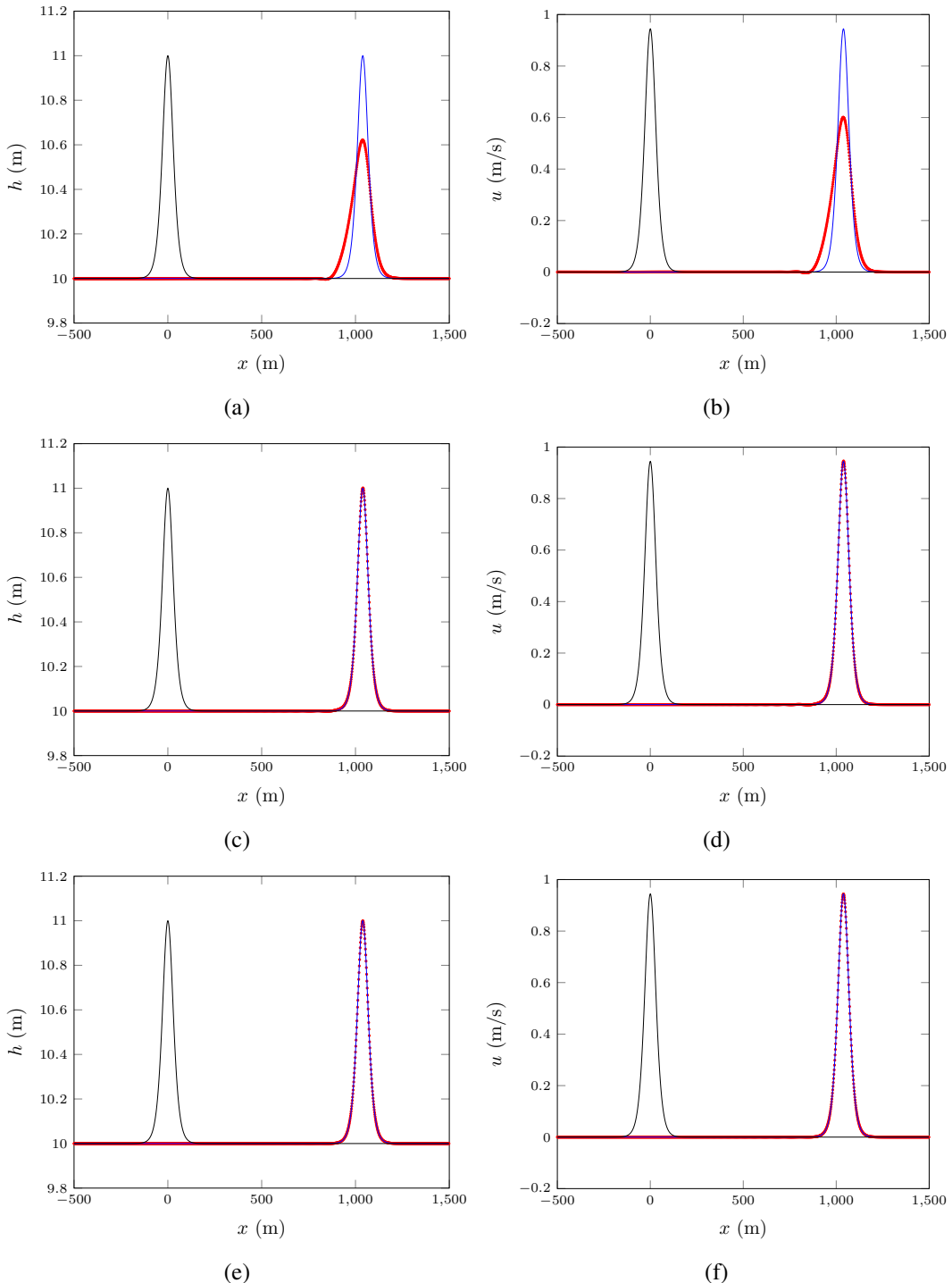


FIG. 2: The first-, second- and third-order simulation of a soliton with $\Delta x = 100/2^6$ m (\bullet) plotted against the analytic solution of (9) (—) with black for $t = 0$ s and blue for $t = 100$ s.

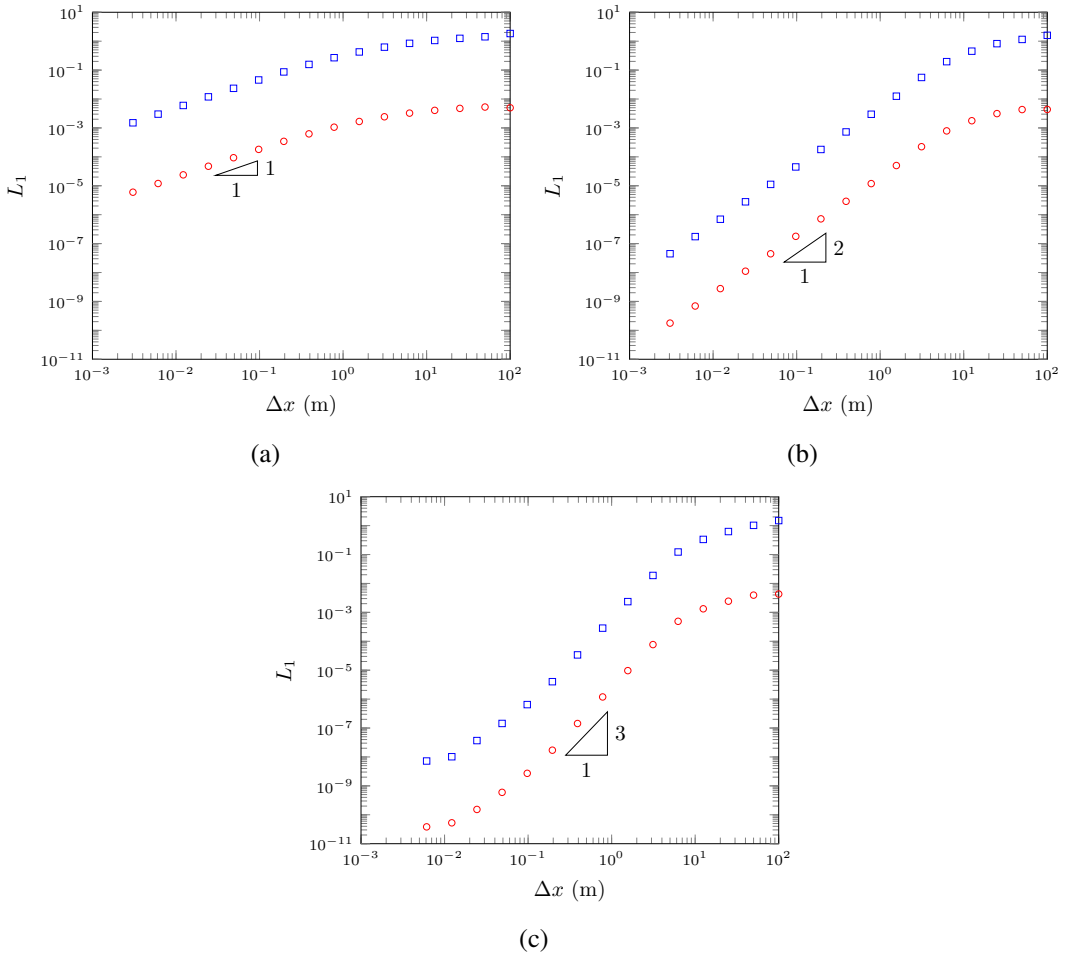


FIG. 3: Convergence of relative error using L_1 norm for analytic soliton solution for both h (\circ) and u (\diamond) for the; (a) first-, (b) second- and (c) third-order methods.

The first-order method has a runtime two orders of magnitude greater than the second- and third-order methods. Which is reasonable because the difference in Δx is also two orders of magnitude. This is computationally restrictive as running practical problems to a reasonable accuracy can have run times that are excessive compared to second- and third-order accurate schemes. Although the second- and third-order methods are more computationally complex than the first-order method this complexity is justified if one wants to numerically solve the Serre equations up to some desired accuracy. This also demonstrates that the second-order method is adequate compared to the third-order method for solving the Serre equations up to some desired accuracy.

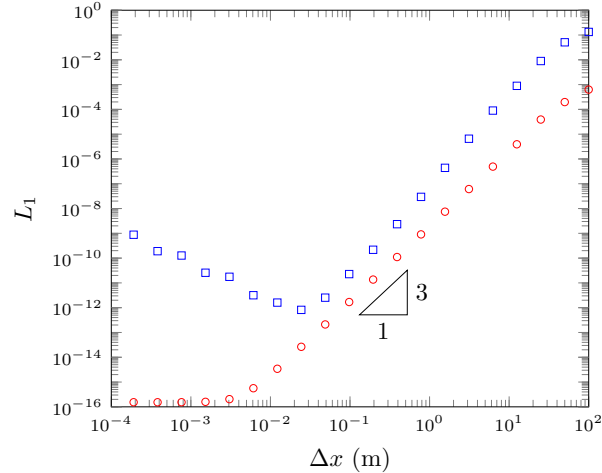


FIG. 4: Convergence of relative error using L_1 norm for analytic soliton solution for both h (\circ) and u (\diamond) over only a single time step

Order	Δx (m)	L_1 relative error for h	L_1 relative error for u	Run Time (s)
First	$100/2^{11}$	$9.32715378271 \times 10^{-5}$	$2.34320597345 \times 10^{-2}$	481.216886997
Second	$100/2^6$	$5.00595847273 \times 10^{-5}$	$1.25175521776 \times 10^{-2}$	2.19665694237
Third	$100/2^5$	$7.681432554 \times 10^{-5}$	$1.89115440455 \times 10^{-2}$	1.3766579628

TABLE 1: Comparison of run times for different order methods to get similar relative error as measured by the L_1 norm for h

321 Figure 3(b) and Figure 3(c) demonstrate that the second- and third-order methods both
 322 have similar errors and Figure 2 shows that these methods resolve the problem well. Therefore,
 323 the extra effort in running a third-order method compared to a second-order method
 324 is not justified in this case. While the effort required to go from a first-order method to a
 325 second-order method is justified since attaining a similar accuracy between them requires
 326 a restrictively small Δx for a first-order method.

327 Segur Laboratory Experiment

328 Hammack and Segur (1978) conducted an experiment that produced rectangular waves
 329 with the stroke of a 0.61m long piston flush with the wall of a wave tank 31.6m in length.
 330 The water height was recorded at 0m, 5m, 10m, 15m and 20m from the edge of the piston
 331 furthest from the wall over time. The quiescent water height h_1 was 0.1m while the stroke
 332 of the piston caused a depression of water which was $h_0 = 0.095$ m deep. To run this as
 333 a numerical simulation the reflected problem was used. Thus the initial conditions were
 334 reflected around the origin and $h_1 - h_0$ was doubled by setting $h_0 = 0.09$ m. The domain

335 was chosen to be from -60m to 60m and the simulation was run for 50s with $\Delta x = 0.01\text{m}$,
 336 $\lambda = 0.2/\sqrt{gh_1}$ m/s which satisfies (8) and $\theta = 1.2$ in the second-order scheme. The results
 337 of this simulation are displayed in Figures 5 - 7.

338 In this experiment for the positive side of the axis the initial depression causes a right
 339 going rarefaction fan and a left going shock. The shocks from both sides then reflect at
 340 the origin and so the shock and the rarefaction fan will travel in the same direction. The
 341 leading wave in all the related figures is the rarefaction fan while the trailing dispersive
 342 waves are the result of the reflected shock.

343 From all the related figures it can be seen that all models show good agreement be-
 344 tween the arrival of the first wave and the period of all the waves. While Figure 5 shows
 345 the first-order method is too diffusive and thus under estimates the heights of the dispersive
 346 waves. Whereas the second- and third-order methods over estimate them. This overesti-
 347 mation can be explained by the Serre equations ignoring viscous effects that may diffuse
 348 the dispersive waves and so the results could be considered as an upper bound on the wave
 349 heights for non-inviscid fluids. Although even without these effects these numerical meth-
 350 ods show good agreement with the experimental data thus validating them to provide a
 351 reasonable representation of rapidly-varying flows. Additionally, it demonstrates that the
 352 oscillations observed by the produced numerical solutions of the Serre equations around
 353 steep gradients are physical and not numerical. In these simulations the numerical oscil-
 354 lations that the second-order method should produce (Zoppou and Roberts 1996) do not
 355 have a significant influence on the physical oscillations.

356 Dam-Break

357 The dam-break problem used by El et al. (2006) to compare their analysis with a
 358 second-order accurate solution of the Serre equations can be defined by

$$359 \quad h(x, 0) = \begin{cases} 1.8m & x < 500m \\ 1.0m & x \geq 500m \end{cases},$$

360 $u(x, 0) = 0.0\text{m/s}.$

361 With $x \in [0\text{m}, 1000\text{m}]$ for $t \in [0\text{s}, 30\text{s}]$. Where $\lambda = 0.01\text{m/s}$ which satisfies (8) and $\theta = 1.2$
 362 for the second-order scheme. This corresponds to sub-critical flow and was a situation
 363 demonstrated in El et al. (2006) and Le Métayer et al. (2010). An example was plotted
 364 for $\Delta x = 100/2^{10}\text{m}$ for all the methods and for $\Delta x = 100/2^{15}\text{m}$ for the first-order method
 365 in Figure 9. To determine if the oscillations that occur in the solution indeed converge
 366 to some limit as $\Delta x \rightarrow 0$ multiple Δx values were run and then the amount of variation
 367 in the solution measured. This measured how oscillatory the solution was and was used
 368 to determine the growth of the oscillations. A common way to measure this is the total

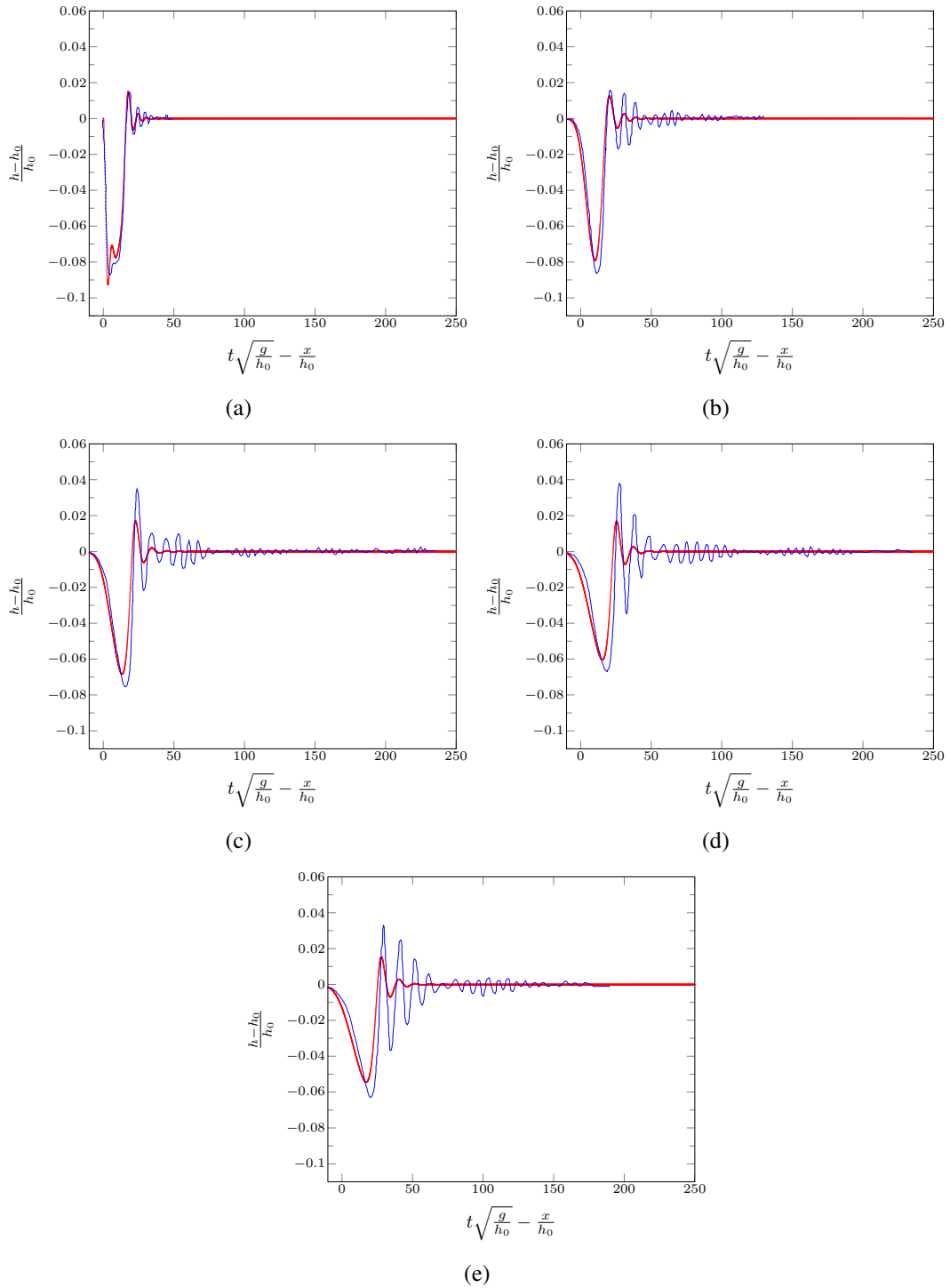


FIG. 5: Comparison of the experimental results (—) against the first-order methods solution (●) at x/h_0 : (a) 0, (b) 50, (c) 100, (d) 150 and (e) 200.

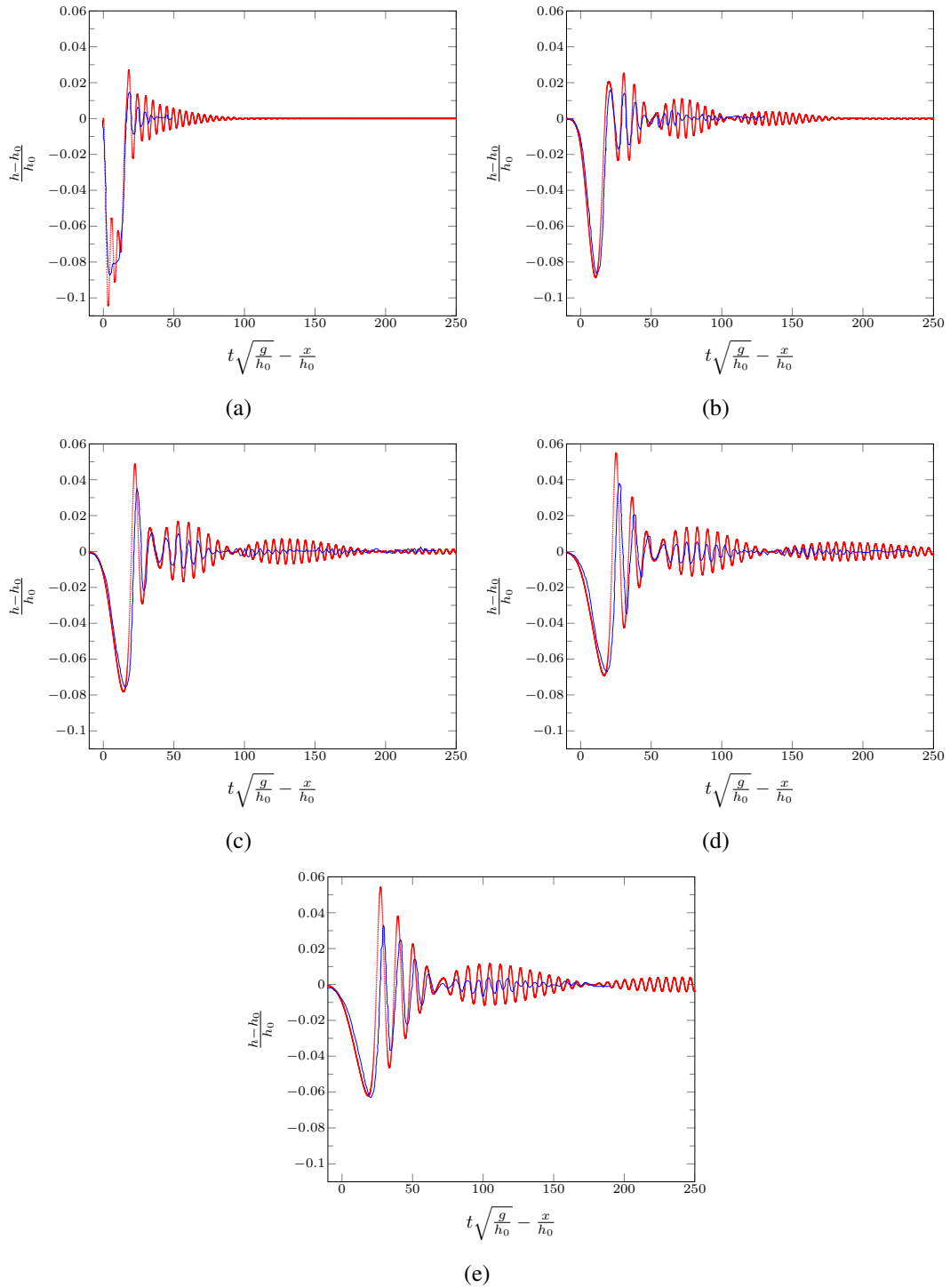


FIG. 6: Comparison of the experimental results (—) against the second-order methods solution (●) at x/h_0 : (a) 0, (b) 50, (c) 100, (d) 150 and (e) 200.

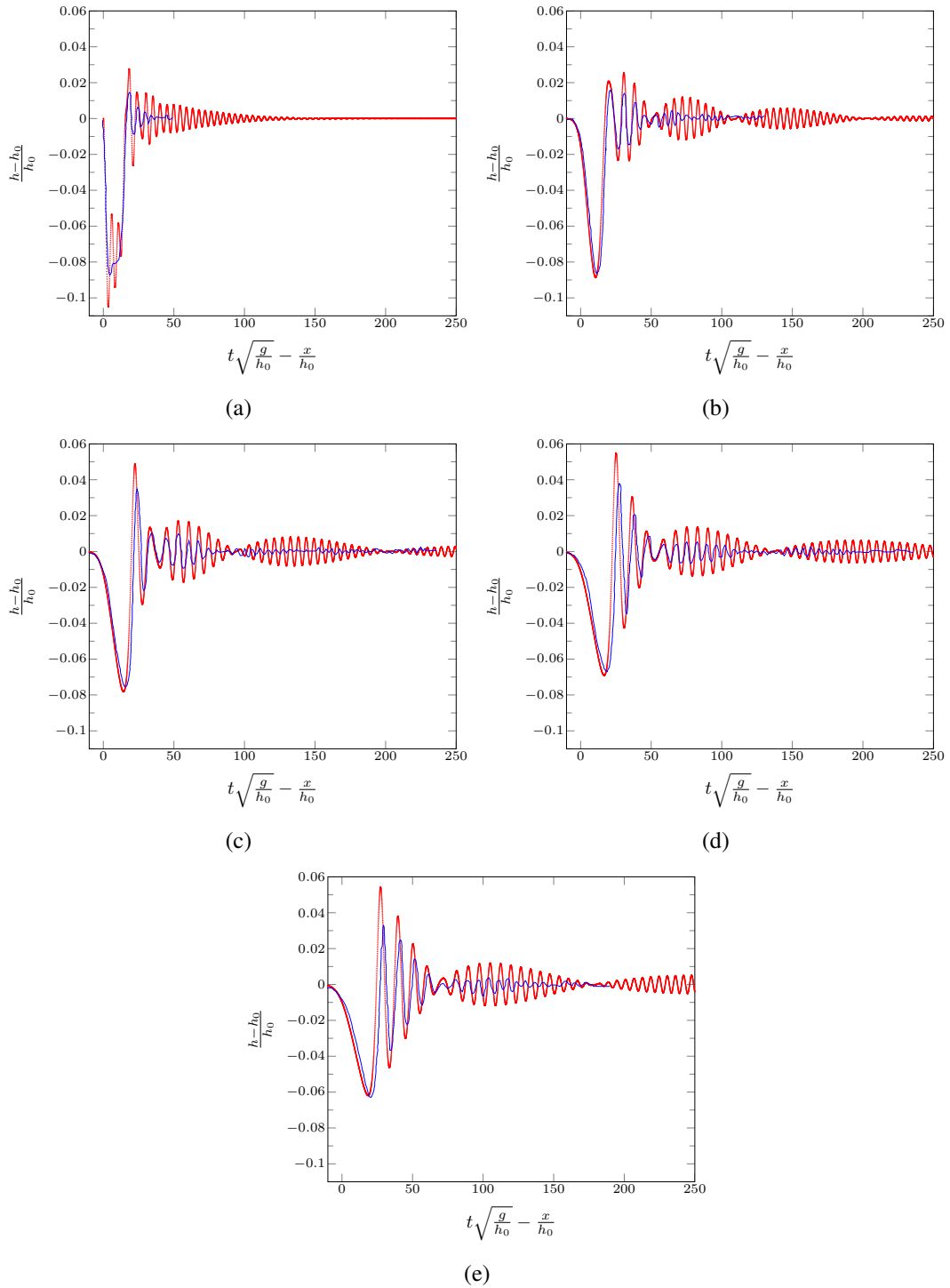


FIG. 7: Comparison of the experimental results (—) against the third-order methods solution (●) at x/h_0 : (a) 0, (b) 50, (c) 100, (d) 150 and (e) 200.

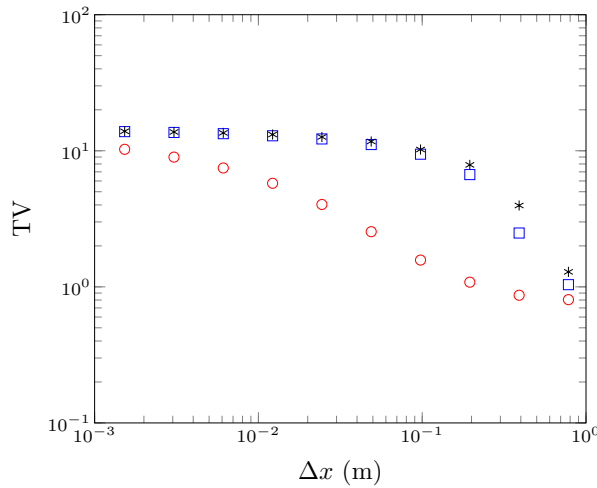


FIG. 8: The change in total variation (TV) over Δx for; (○) first-, (□) second-, and (*) third-order methods.

369 variation TV (LeVeque 2002) which for \mathbf{q} is given by

370

$$371 \quad TV(\mathbf{q}) = \sum_{\forall i>1} |q_i - q_{i-1}|.$$

372 If the solution does indeed converge then the TV must at some point plateau, bounding
 373 the oscillations. This was indeed the findings of the experiments as can be seen by Fig-
 374 ure 8. The TV increases as Δx decreased because the models resolved more dispersive
 375 waves. As Δx decreased further the TV plateaued and so the size and number of oscilla-
 376 tions was bounded. Therefore, the method has not become unstable which supports the
 377 argument that the numerical methods do not introduce non-physical oscillations in the so-
 378 lution. Under this measure the second-order method converges rapidly to the solution of
 379 the third-order method.

380 These solutions compare very well to the findings in El et al. (2006) with both the
 381 second- and third-order methods resolving the oscillations around the “contact discontinu-
 382 ity”(El et al. 2006) between the rarefaction fan and the shock. In Le Métayer et al. (2010)
 383 it was reported that for their first-order method such oscillatory behaviour was not seen.
 384 However, for the first-order method proposed in this paper when $\Delta x = 100/2^{15}$ it was
 385 resolved as in Figure 9(d). This validates the findings in El et al. (2006). Interestingly this
 386 is a much higher resolution than one needs to represent the waves themselves. It appears
 387 that the behaviour of the dispersive waves around a steep gradient is sensitive to diffusion
 388 so that even though the first-order method in Figure 9(a) heuristically had enough cells to

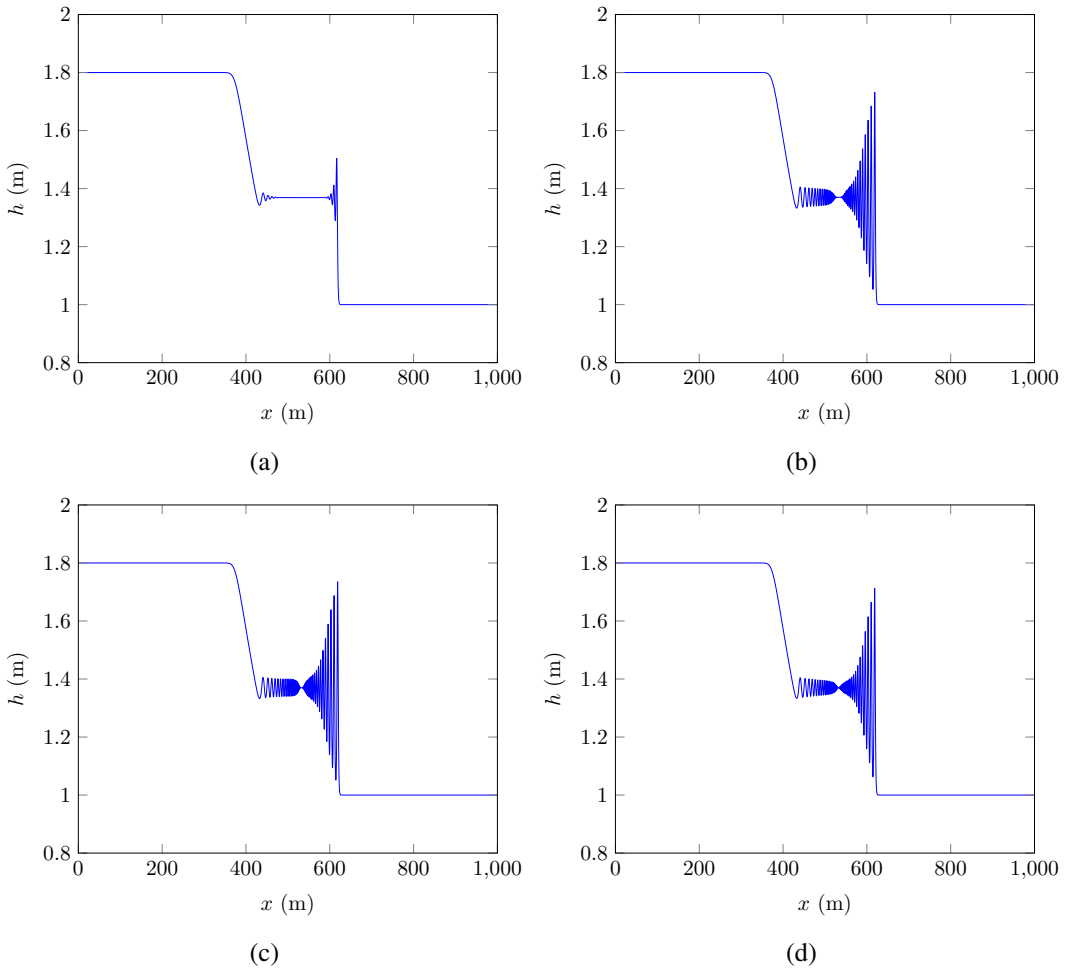


FIG. 9: Solution of the dam-break problem using the (a) first-, (b) second- and (c) third-order method with $\Delta x = 100/2^{10}\text{m}$. As well as a (d) first-order method with $\Delta x = 100/2^{15}\text{m}$.

389 resolve most of the wave train, due to strong diffusion hardly any of the wave train was
 390 resolved.

391 There is a good agreement between the second- and third-order simulations of the dam-
 392 break problem as can be seen in Figures 9(b) and 9(c). Although more oscillations are
 393 resolved by the third-order method over the second-order method, there is no significant
 394 change in the resolved behaviour of this problem between the two methods. As noted in the
 395 introduction second-order accurate numerical schemes are dissipative; since the diffusive
 396 third-order method resolved the same oscillations it was demonstrated that none of the

397 dissipative errors significantly polluted the wave train and for this problem the second-
398 order accurate scheme is capable of resolving the problem.

399 **CONCLUSIONS**

400 First-, second- and third-order hybrid finite difference-volume methods were devel-
401 oped to solve the Serre equations written in conservative law form. The methods were
402 then tested and validated. Firstly the order of the methods were all verified, secondly
403 the methods steep gradient handling capability was validated by comparison with experi-
404 mental data. Thirdly the behaviour of the solutions matched previous findings in El et al.
405 (2006). Thus it can be concluded that these methods are all valid and they properly handle
406 steep gradients. It was also demonstrated that for these equations although second-order
407 is not as accurate as third-order it still provides a satisfactory method for reasonable Δx
408 unlike the first-order method which due to the introduction of large numerical diffusion
409 requires computationally restrictive Δx to produce satisfactory accuracy. Therefore; prac-
410 tical problems which contain steep gradients require at least a second-order method to
411 solve the Serre equations.

412 **ACKNOWLEDGEMENTS**

413 Dr David George, Cascades Volcano Observatory, U.S. Geological Survey for providing
414 the rectangular wave data.

415 **REFERENCES**

- 416 Antunes do Carmo, A., Seabra-Santos, F. J., and Almeida, A. B. (1993). “Numerical solution
417 of the generalized Serre equations with the MacCormack finite-difference scheme.” *International Journal for Numerical Methods in Fluids*, 16(8), 725–738.
- 418 Bonneton, P., Chazel, F., Lannes, D., Marche, F., and Tissier, M. (2011). “A splitting approach for the fully nonlinear and weakly dispersive Green-Naghdi model.” *Journal of Computational Physics*, 230(4), 1479–1498.
- 419 Carter, J. D. and Cienfuegos, R. (2011). “Solitary and cnoidal wave solutions of the Serre
420 equations and their stability.” *European Journal of Mechanics B/Fluids*, 30(3), 259–268.
- 421 Chazel, F., Lannes, D., and Marche, F. (2011). “Numerical simulation of strongly nonlinear
422 and dispersive waves using a Green-Naghdi model.” *Journal of Scientific Computing*, 48(1-3), 105–116.
- 423 Cienfuegos, R. and Barthélemy, E. and Bonneton, P. (2006). “A fourth-order compact finite
424 volume scheme for fully nonlinear and weakly dispersive Boussinesq-type equations.
425 Part i: model development and analysis.” *International Journal for Numerical Methods
426 in Fluids*, 51, 1217–1253.
- 427 Cienfuegos, R. and Barthélemy, E. and Bonneton, P. (2007). “A fourth-order compact finite
428 volume scheme for fully nonlinear and weakly dispersive Boussinesq-type equations.
429 Part ii: Boundary conditions and validation.” *International Journal for Numerical
430 Methods in Fluids*, 53, 1423–1455.
- 431 Courant, R., Friedrichs, K., and Lewy, H. (1928). “Über die partiellen Differenzengleichungen
432 der mathematischen physik.” *Mathematische Annalen*, 100(1), 32 – 74.
- 433 Dutykh, D., Clamond, D., Milewski, P., and Mitsotakis, D. (2011). “Finite volume and
434 pseudo-spectral schemes for the fully nonlinear ‘irrotational’ Serre equations.” *Arxiv*,
435 24(5), 0 – 25.
- 436 El, G., Grimshaw, R. H. J., and Smyth, N. F. (2006). “Unsteady undular bores in fully
437 nonlinear shallow-water theory.” *Physics of Fluids*, 18(027104).
- 438 Godunov, S. K. (1959). “A difference method for numerical calculation of discontinuous
439 solutions of the equations of hydrodynamics.” *Matematicheskii Sbornik*, 89(3), 271–
440 306.
- 441 Gottlieb, S., Ketcheson, D. I., and Shu, C. W. (2009). “High order strong stability preserving
442 time discretizations.” *Journal of Scientific Computing*, 38(3), 251–289.
- 443 Green, A. E. and Naghdi, P. M. (1976). “A derivation of equations for wave propagation
444 in water of variable depth.” *Journal of Fluid Mechanics*, 78(2), 237–246.

- 449 Hammack, J. L. and Segur, H. (1978). “The Korteweg-de Vries equation and water waves.
 450 Part 3. Oscillatory waves.” *Journal of Fluid Mechanics*, 84(2), 337–358.
- 451 Koren, B. (1993). “A robust upwind discretization method for advection, diffusion and
 452 source terms.” *Notes on Numerical Fluid Mechanics*, Vol. 45, Centrum voor Wiskunde
 453 en Informatica, Amsterdam.
- 454 Kurganov, A., Noelle, S., and Petrova, G. (2002). “Semidiscrete central-upwind schemes
 455 for hyperbolic conservation laws and Hamilton-Jacobi equations.” *Journal of Scientific
 456 Computing, Society for Industrial and Applied Mathematics*, 23(3), 707–740.
- 457 Lannes, D. and Bonneton, P. (2009). “*Physics of Fluids*, 21(1), 16601–16610.
- 458 Le Métayer, O., Gavrilyuk, S., and Hank, S. (2010). “A numerical scheme for the Green-
 459 Naghdi model.” *Journal of Computational Physics*, 229(6), 2034–2045.
- 460 LeVeque, R. (2002). *Finite Volume Methods for Hyperbolic Problems*, Vol. 54 of *Cam-
 461 bridge Texts in Applied Mathematics*. Cambridge University Press.
- 462 Li, M., Guyenne, P., Li, F., and Xu, L. (2014). “High order well-balanced CDG-FE meth-
 463 ods for shallow water waves by a Green-Naghdi model.” *Journal of Computational
 464 Physics*, 257, 169–192.
- 465 Mitsotakis, D., Ilan, B., and Dutykh, D. (2014). “On the Galerkin/Finite-Element Method
 466 for the Serre Equations.” *Journal of Scientific Computing*, 61(1), 166–195.
- 467 Serre, F. (1953). “Contribution à l’étude des écoulements permanents et variables dans les
 468 canaux.” *La Houille Blanche*, 6, 830–872.
- 469 Su, C. H. and Gardner, C. S. (1969). “Korteweg-de Vries equation and generalisations.
 470 III. Derivation of the Korteweg-de Vries equation and Burgers equation.” *Journal of
 471 Mathematical Physics*, 10(3), 536–539.
- 472 Zoppou, C. (2014). “Numerical solution of the One-dimensional and Cylindrical Serre
 473 Equations for Rapidly Varying Free Surface Flows.” Ph.D. thesis, Australian National
 474 University, Acton ACT 2601 Australia.
- 475 Zoppou, C. and Roberts, S. (1996). “Behaviour of finite difference schemes for advection
 476 diffusion equations.” *Technical Report Mathematics Research Report No.MRR 062-96*.